Originally published in *Proceedings of the Fifth International Workshop on Compressible Turbulent Mixing*, ed. R. Young, J. Glimm & B. Boston.
ISBN 9810229100, World Scientific (1996).

A Numerical Study of Shock-Acceleration of a Diffuse Helium Cylinder

Jeffrey A. Greenough[1] and Jeffrey W. Jacobs[2]

[1] Computational Sciences and Engineering
Lawrence Livermore Nat'l Lab.
Livermore, CA 94550

[2] Aerospace and Mechanical Engineering
University of Arizona
Tucson, AZ 85721

Abstract.
The development of a shock-accelerated diffuse Helium cylindrical inhomogeneity is investigated using a new numerical method. The new algorithm is a higher-order Godunov implementation of the so-called multi-fluid equations. This system correctly models multiple component mixtures by accounting for differential compressibility effects. This base integrator is embedded in an implementation of adaptive mesh refinement (AMR) that allows efficient increase in resolution by concentrating the computational effort where high accuracy, or increased resolution, are required. Qualitative and quantitative comparison with previous experimental data is excellent. The simulations show that counter-sign vortex blobs are deposited in the jet core by baroclinic generation of the curved shock wave as it traverses the jet. This vorticity deposition occurs over time scales that scale with the shock passage time ($\sim 10\mu$sec). Three phases of development are identified and characterized. The first is the weak deformation (WD) phase, where there is weak distortion of the Helium jet due to weak vorticity induced velocity effects. The second phase is the strong deformation (SD) phase where there is large distortion for the jet and the vortex blobs due to large induced velocity effects. The last is a relaxation/reorganization (RR) phase where the vorticity field is reorganized into point-like vortex pair.

1 Introduction

The evolution of interfaces accelerated by shock waves has been the focus of investigations for many years. This class of problem has applications in such disparate fields as inertial confinement fusion (ICF) and high-speed combustion. The literature is rich in studies on the stability of plane interfaces [1], [2], and [3]. The stability of curved interfaces has received similar attention culminating with the study of [4], where cylindrical or spherical shapes, constructed from soap bubbles or nitrocellulose membranes, where

filled with either a light or heavy gas and then accelerated by a shock wave. This last study and the previous works relied on such membranes to separate gases. A different class of experiment on acceleration of gaseous cylinders was developed by [6] and [5] that was free from the effect of membranes and used a planar laser induced fluorescence (PLIF) technique for obtaining excellent visualization of the flow and quantitative information regarding mixing.

The present simulations use a high resolution adaptive method designed for multi-fluid flows with initial mixed layers. In this paper, the development of the Helium mole fraction and vorticity field will be examined. Extensive comparisons with experimental data have also been completed as well as development of a new conceptual model describing this flow, but cannot be described here due to space limitations.

2 Multi-fluid System and Numerical Method

The equations used for this study are the so-called multi-fluid equations as developed by [7] and also described in [8]. This system is based on a volume-of-fluid approach, where the fraction of a cell volume occupied by a distinguished fluid is actually followed during flow evolution. The basic assumptions in this approach are that there is pressure equilibrium within a cell, there is a single velocity vector for both fluids and that all changes of state are adiabatic. The equations are given as

$$\frac{\partial f^\alpha}{\partial t} + \nabla \cdot (\boldsymbol{u} f^\alpha) = f^\alpha \frac{\hat{\Gamma}}{\Gamma^\alpha} \nabla \cdot \boldsymbol{u} \tag{2.1}$$

$$\frac{\partial}{\partial t} (f^\alpha \rho^\alpha) + \nabla \cdot (\boldsymbol{u} f^\alpha \rho^\alpha) = 0 \tag{2.2}$$

$$\frac{\partial \rho \boldsymbol{u}}{\partial t} + \nabla \cdot (\boldsymbol{u}\boldsymbol{u}\rho) + \nabla p = 0 \tag{2.3}$$

$$\frac{\partial}{\partial t} (f^\alpha \rho^\alpha E^\alpha) + \nabla \cdot (\boldsymbol{u} f^\alpha \rho^\alpha E^\alpha) + p f^\alpha \frac{\hat{\Gamma}}{\Gamma^\alpha} \nabla \cdot \boldsymbol{u} + f^\alpha \frac{\rho^\alpha}{\rho} \boldsymbol{u} \cdot \nabla p = 0 \tag{2.4}$$

where f^α, ρ^α, and E^α are the volume fraction, density, and total energy density of fluid component α. The volume fraction is defined as $f^\alpha = \Lambda_\alpha / \Lambda$ where Λ is the volume of the cell and Λ_α is the volume of the cell occupied by fluid α. Γ^α is the sound speed gamma for fluid α, and $\hat{\Gamma} = 1/\sum_\alpha (f^\alpha/\Gamma^\alpha)$ represents fraction weighted Γ for the mixture.

The pressure that appears in the above system is defined to be a thermodynamically consistent pressure and defined as $p = \sum_i \hat{\Gamma} \left(f^i p^i / \Gamma^i \right)$, where p^α is the partial pressure of component α. Note that the formulation is sufficiently general to allow real gas EOS systems described by pressure given as a function of density and internal energy.

The solution procedure for the system is a higher-order Godunov method following that of [9] and detailed in [10]. This base integrator for the multi-fluid system is embedded within an implementation of adaptive mesh refinement (AMR). This methodology is based on the original work of [11] and later [12]. This is a means for managing a refined grid hierarchy composed of logically rectangular grid patches that allows for efficient increases in resolution by focusing the computational accuracy where errors are deemed large, or in regions where high resolution is required.

3 Problem Setup

The initial conditions for this problem are taken from [6]. The shock wave Mach number is 1.094 in air. In [13], a Raleigh scattering technique is used to measure the actual molar concentrations of Helium. It shows the initial profile is Gaussian in shape with a core concentration of approximately 80% Helium. The initial half radius is set as, $r_{half} = 0.2$, where it is defined as the distance where the Helium mole fraction is half the center value. The density ratio between air and Helium is $\rho_{\text{Helium}}/\rho_{\text{air}} = .138$.

The computational domain is 9cm wide by 27cm long with a base grid of 36 cells wide by 108 cells long. There are two levels of refinement where the first level is a factor of 4 more refined than the base grid and the second level is a factor of 8 more refined than the first level of refinement. This gives an effective grid resolution of $\Delta x_{fine} = \Delta y_{fine} = 0.0078125$cm. The shock is initialized in air a distance of $3r_{half}$ from the jet. All boundaries are inflow/outflow type.

4 Results and Discussion

4.1 Flow Visualization

Figures 1 and 2 shows the evolution of the mole fraction of Helium and the development of the vorticity field, respectively. Figure 1(a) shows the initial conditions and the initial mixed layer. At 88μsec, figure 1(b), there is a flattening of the jet and a generally weak deformation of its original circular structure. From here out to about 400μsec, spanned in time by figures 1(c) through (f), there is strong deformation of the jet as it is inverted and transformed into the vortex pair. After 400μsec, from figure 1(g) on, the flow evolves as a well defined vortex pair. Comparing these results with those given in [6], the agreement is exceptional.

Based on these observations and for ease and clarity of later exposition, we define three phases of development. The first is the weak deformation phase (WD) that occurs over short times out to about 90μsec. The second is the strong deformation phase (SD) that occurs after WD out to about 400μsec. The last is the relaxation/reorganization (RR) phase that occurs after SD.

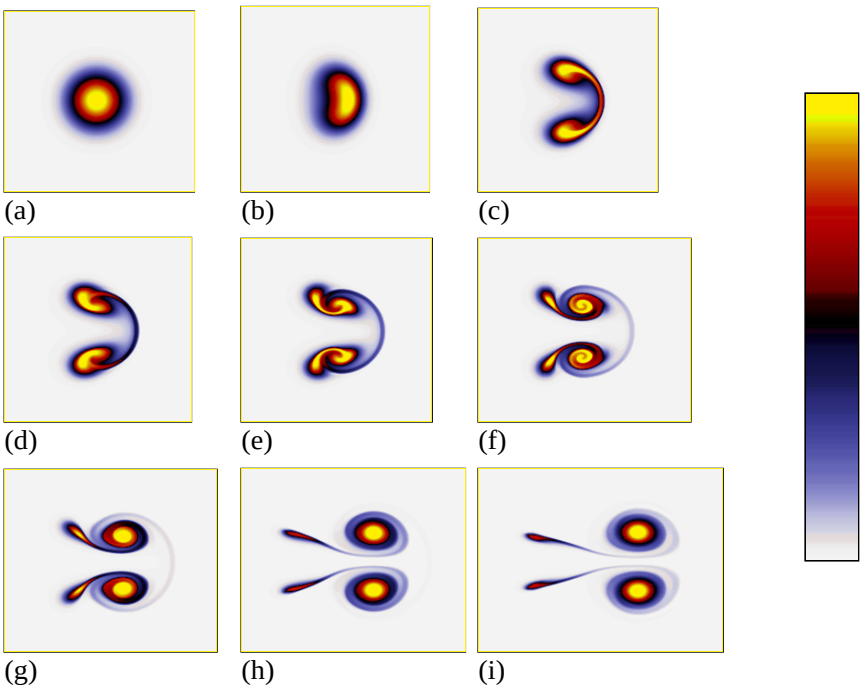

Figure 1: A sequence of the computed Helium mole fraction evolution. Note that the shock arrival time at the jet is approximately 40μsec and all times reported are relative to the start of the calculation. (a) The initial jet, (b) 88μsec, (c) 202μsec, (d) 259μsec, (e) 318μsec, (f) 436μsec, (g) 561μsec, (h) 943μsec, (i) 1182μsec. The shock moves from left to right. The color bar to the right varies highest to lowest values from top to bottom.

In the vorticity time sequence, figure 2(a) shows the shock, still essentially planar, leaving positive (in the upper half plane) vorticity behind it. By 66μsec, figure 2(b), the shock is well out of the jet core and two counter-sign circular vortex blobs are seen located in the jet core. During the WD phase, the vortex blobs remain essentially undistorted. This is due to the fact that vorticity induced velocity effects are very weak during the WD phase. Also, the blobs are deposited in the jet core over a time scale that scales with the shock passage time ($\sim 10\mu$sec). It turns out that as the shock traverses the density stratification that the peak baroclinic production (by two orders of magnitude relative to all other values in the field) occurs at the curved shock. That means that at each instant in time, as the shock progresses across the jet that it acts as a strong source of vorticity. The result is what is shown in figure 2(b); the vortex blob pair. There is secondary production in the post shock region, but over times on the order of the shock passage time, these are weak secondary effects. During the SD phase however, there are large induced velocity effects that distort and stretch the vortex blobs

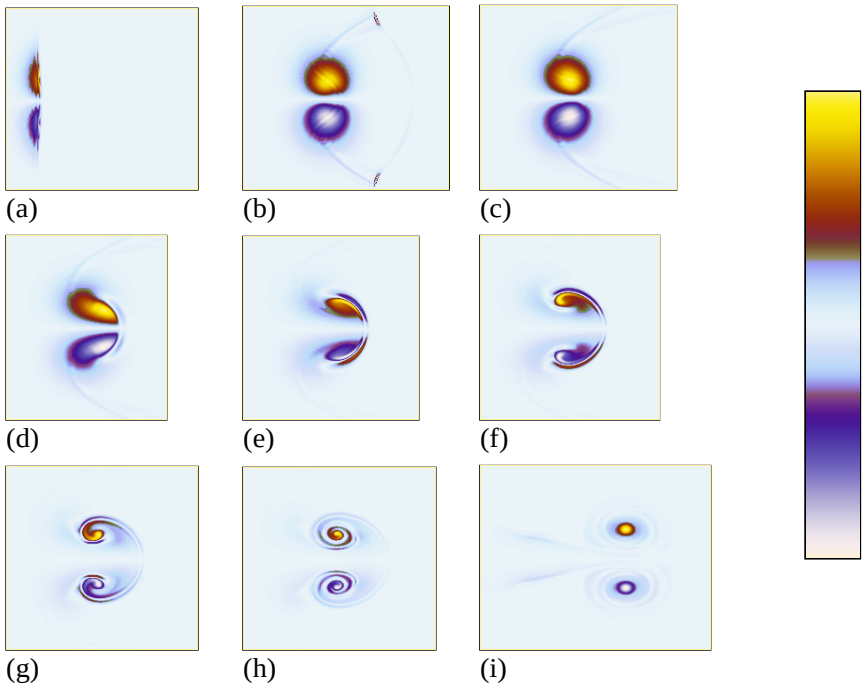

Figure 2: A sequence of the vorticity evolution. Note that the shock arrival time at the jet is approximately 40μsec and all times reported are relative to the start of the calculation. (a) 44μsec, (b) 66μsec, (c) 88μsec, (d) 141μsec, (e) 202μsec, (f) 259μsec, (g) 318μsec, (h) 436μsec, (i) 1182μsec. The shock moves from the left to right. The color bar to the right is centered with respect to the data. Values vary highest positive to highest negative from top to bottom.

into continuous finite thickness sheets of vorticity. These sheets are swirled around and reorganize, at later times, into a point-like vortex pair. Note that during the SD phase, there is strong counter-sign vorticity appearing that is also oriented in sheets, ahead of the distorted blob. Although not shown here, this counter-sign production acts to modulate the overall circulation as it relaxes to a near constant value. During the late time relaxation phase, the signed baroclinic production is essentially in balance leading to the circulation approaching a constant state.

The development of this flow is seen to be determined by the interaction and evolution of the vortex blobs. Once they are present in the flow, they at first interact weakly (during WD), then interact strongly (during SD) as they change from blobs, to point-like vortices (during RR). During the course of the transformation of the vorticity field, the Helium jet undergoes a similar transformation as shown above. From a modeling point of view, this flow could be accurately depicted by the development of a vortex blob pair in an essentially circular helium jet (slightly flattened on the upstream

side in reality). The subsequent development could be dictated by their interaction and reorganization/relaxation to point vortices. The free parameters could include blob half-width, strength, and spacing. Also, there is the degree of flattening on the upstream side of the jet that could be taken into account.

4.2 Vortex Blob Deposition

Figure 3 shows a composite of the vorticity, the baroclinic generation, and the total density at two instants in time separated by 4μsec. The figures from top to bottom are aligned spatially. The three frames on the left are all at 49μsec and the three on the right are all at 53μsec. In the frames on the left, the shock wave is curved and the shock leading edge is coincident with the peak Helium concentration.

In the vorticity field at 49μsec, figure 3(a), the early stages of positive and negative vortices are seen just behind the curved shock. The baroclinic production field at this time, figure 3(c), shows the peak values are located at the curved portion of the shock wave within the jet. Note that these maxima are about 2 orders of magnitude greater than all other values in the field. This production along the curved shock wave is the mechanism for generating the vortex blobs. At each instant in time, the baroclinic generation due to the curved shock in a stratified density field acts as a strong source term in the vorticity evolution equation (positive in the upper half plane and negative in the lower half plane). The result over the time of the shock passage is the counter-signed vortex blobs as shown in Figure 3(d). The peak vorticity values occur in the blobs. Note that the baroclinic generation behind the shock wave within the jet only weakly modulates the blob vorticity distribution. By 53μsec the shock has passed beyond r_{half} and the peak generation of circulation is over.

References

[1] R.D. Richtmyer 1960 Taylor instability in shock acceleration of compressible fluids. *Commun. Pure Appl. Math* **23**, 297-319.

[2] E.E. Meshkov 1969 Instability of the interface of two gases accelerated by a shock wave. *Izv. Akad. Nauk. SSSR Mekh. Ahidk. Gaza* **4**, 1151-157 [Russian: *Izv. Acad. Sci. USSR Fluid Dyn.* **4**, 101-104.

[3] Zaitsev, S.G., Lazareva, E.V., Chernukha, V.V., & Belyaev, V.M. 1985 Experimental investigation of the hydrodynamic instability of the interface between media of different density in an acceleration field. Translated from *Teplofzika Vysokikh Temperatur* **23**, 535-541.

[4] Haas, J.-F. & Sturtevant, B. 1987 Interaction of weak shock waves with cylindrical and spherical inhomogeneities. *J. Fluid Mech.*, **181**, 42-76.

[5] Jacobs, J.W. 1992 Shock-induced mixing of a light-gas cylinder. *J. Fluid Mech.* **234**, 629-649.

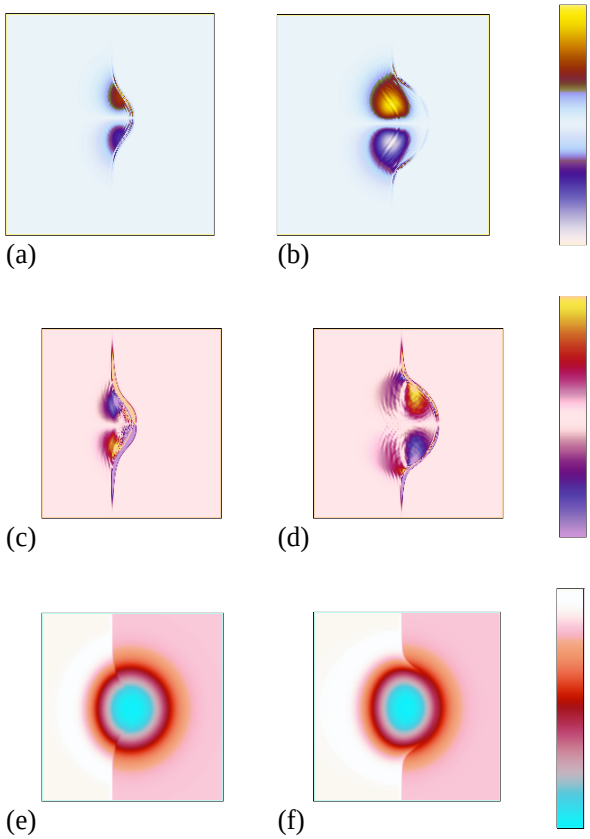

Figure 3: A short time composite sequence at 49μsec of the (a) vorticity, (c) baroclinic generation, and (e) total density and at 53μsec of the (b) vorticity, (d) baroclinic generation, and (f) total density. Note that the shock wave moves from left to right and the figures are aligned spatially.

[6] Jacobs, J.W. 1993 The dynamics of shock accelerated light and heavy gas cylinders. *Phys. Fluids* A **5**, 2239-2247.

[7] Colella, P., Ferguson, R.E., Glaz, H.M. 1995 Multi-fluid algorithms for Eulerian finite difference methods. Manuscript.

[8] Puckett, E.G. & Saltzman, J.S. 1992 A 3-d adaptive mesh refinement algorithm for multi-material gas dynamics. *Physica* D **60**, 84-104.

[9] Colella, P. 1984 A direct Eulerian MUSCL scheme for gas dynamics. *SIAM J. Sci. Stat. Comput.* **6**, 104-117.

[10] Greenough, J.A., Bell, J.B., Colella, P. 1995 An adaptive multi-fluid interface-capturing method for compressible flows in complex geometry. AIAA Paper 95-1718.

[11] Berger, M.J. & Oliger, J. 1984 Adaptive mesh refinement for hyperbolic partial differential equations. *J. Comput. Phys.* **53**, 484-512.

[12] Berger, M.J. & Colella P. 1989 Local adaptive mesh refinement for shock hydrodynamics. *J. Comput. Phys.*, **82**, 64-84.

[13] Budzinski, J.M. 1992 Planar Rayleigh scattering measurements of shock enhanced mixing. Doctoral dissertation. California Institute of Technology.